Innovative orbit determination algorithms for a complete debris catalogue in the upper LEO region.

Linda Dimare[(1)], Andrea Milani[(1)], Davide Farnocchia[(1)] , Alessandro Rossi[(2)], Fabrizio Bernardi[(1)]

[(1)]*Dipartimento di Matematica, Università di Pisa,*
Largo B.Pontecorvo, 5, 56127, Pisa, Italy
Email: dimare@mail.dm.unipi.it, milani@dm.unipi.it, farnocchia@mail.dm.unipi.it, bernardi@adams.dm.unipi.it

[(2)]*IFAC-CNR & ISTI-CNR*
CNR – Area della Ricerca di Firenze
Via Madonna del Piano, 10, 50019, Sesto Fiorentino, Firenze, Italy
Email: alessandro.rossi@isti.cnr.it

ABSTRACT

We present the results of a large scale simulation, reproducing the behaviour of a data centre for the build-up and maintenance of a complete catalogue of space debris in the upper part of the low Earth orbits region (LEO). The purpose is to determine the performances of a network of advanced optical sensors, through the use of the newest orbit determination algorithms developed by the Department of Mathematics of Pisa (DM). Such a network has been proposed to ESA in the Space Situational Awareness (SSA) framework by Carlo Gavazzi Space SpA (CGS), Istituto Nazionale di Astrofisica (INAF), DM and Istituto di Scienza e Tecnologie dell'Informazione (ISTI-CNR).

The conclusion is that it is possible to use a network of optical sensors to build up a catalogue containing more than 98% of the objects with perigee height between 1100 and 2000 km, which would be observable by a radar system as envisaged for the ESA SSA project. It is also possible to maintain such a catalogue within the accuracy requirements motivated by collision avoidance, and to detect catastrophic fragmentation events. However, such results depend upon specific assumptions on the sensor and on the software technologies.

INTRODUCTION

In the context of the European program SSA, the aim of the project SARA-Part I *Feasibility study of an innovative system for debris surveillance in LEO regime* was to demonstrate the feasibility of a European network based on optical sensors, capable of complementing the use of UHF radars for the identification and cataloguing of debris in the high part of the LEO region, to lower the requirements on the radar system in terms of power and performances. The proposal relied on the definition of a wide-eye optical instrument able to work in high LEO zone and on the development of new orbit determination algorithms, suitable for the kind and amount of data coming from the surveys targeting at LEOs.

A new algorithm, based on the first integrals of the Kepler problem, was developed by DM to solve the critical issue of LEOs orbit determination. Standard methods, such as Gauss' [7], require at least three observations per pass in order to compute a preliminary orbit, while the proposed algorithm needs only two exposures, observed at different passes. This results in a significant reduction of the number of required telescopes, thus of the cost of the entire system. In addition, the proposed method takes into account the nodal precession due to the quadrupole term of the Earth geopotential. Because of the low altitude of the orbits and the availability of only one exposure per pass, this effect is not negligible and it must be considered since the first step of preliminary orbit computation.

The aim was to perform a realistic simulation. Thus in addition to the correlation and orbit determination algorithms, all the relevant elements of the optic system were considered: the telescope design, the network of sensors, the observation constraints and strategy, the image processing techniques. Starting from the ESA-MASTER2005 population model, CGS provided us with simulated observations, produced taking into account an advanced design for the optical sensors. The provided data were processed with our new orbit determination algorithms in three phases: catalogue build-up, orbit improvement and fragmentation analysis.

OBSERVABILITY AND NETWORK DEFINITION

To observe debris some conditions must be verified, which are dependent on the object orbit parameters, the observatory location and the seasonal factors. The first limitations derive from geometrical constraints. An orbiting object at a fixed altitude is visible only up to a given distance from a station, beyond which the object is under the minimum needed elevation, typically 15 deg. An high LEO has, on average, 4 passes/day above the required elevation, when observed from a station at low latitudes (within 30 deg). Note that these constraints apply also to a radar sensor.

The main difference with radar arises because of the geometry of sunlight. For optical observations the ground station must be in darkness, with the Sun at least 10-12 deg below the horizon, so that the sky is dark enough to begin operations. This happens on average about 30-60 min after sunset and before sunrise, but it strongly depends on the latitude and the season of the station. Moreover, the orbiting object must be in sunlight and the atmosphere must be clear, without dense clouds and light pollution.

Fig. 1 shows the shadow cone for a nearly tropical station (latitude 27 N), on March 20th, at the local solar time 19 h. The red line represents the boundary of Earth shadow at 1400 km above the ground. The Earth shadow region is grey. The circles represent the iso-elevation directions of the sky above the horizon of the location, which is represented by the outer circle. The centre of the plot is the local zenith. The labelled lines (30, 60, 90 and 120) represent the iso-phase curves for objects at 1400 km above the ground; the apparent magnitude of the objects strongly depends upon the phase, e. g., a phase 90 deg results in an increase by >3 magnitudes with respect to phase 0. The plot shows that the regions with smaller phase angles are the ones close to the Earth shadow boundary. The best conditions to observe objects at the smallest possible phase angles are during the minutes just after sunset or before sunrise, when the shadow region is smaller. Very small objects, down to some centimetres, are detectable only when they are very close to the Earth shadow boundary and during the short observability window either after sunset or before sunrise.

The meteorological constraints can be handled by having stations far enough to have low meteorological correlation. An high inclination object is more likely to be observed by an high latitude station. To guarantee a good coverage in all seasons both North and South high latitude stations are required. By drawing a shadow cone figure like Fig. 1, it is easy to see that the larger is the latitude, the smaller is the obstruction to observability due to the shadow cone. However, an higher latitude implies shorter hours of darkness in summer and bad weather in winter, thus intermediate latitude stations, around 45 deg, are the best compromise. The network needs to be spread over the world to increase the efficiency of the system, but there are geopolitical and logistic constraints to be considered: availability to Europe, orography, electrical power, airports, and so on. The optical station network devised for our simulations was made of 7 stations: 3 in the equatorial area, which are Teide (Canary islands), Hao (French Polynesia) and New Norcia (Australia); 2 in the Northern hemisphere, which are Gran Sasso (Italy) and Pico de Vara (Azores); 2 in the Southern hemisphere, which are Falkland Islands and Malargue (Argentina). The network was chosen using the information on the meteorological conditions, which were simulated on the basis of the actual public-domain weather satellite data, obtained mainly from the ISCCP (NASA) project (http://isccp.giss.nasa.gov/index.html).

ASSUMPTIONS ON THE OPTICAL SENSORS

We assumed a large field telescope based upon a Fly-Eye technology, whose architecture and design is under study in the ESA *CO-V Telescopes Analysis and Design* study, see [4]. The telescope has a primary mirror of 110 cm diameter, with equivalent aperture of 100 cm, and it has the capability of fast motion. The field of view covers 45 deg^2. The telescope is adequate to perform both survey and follow-up observations. Moreover, the "idle time" in LEO observations due to the Earth shadow can be exploited to observe objects in higher orbits with only software changes, typically with longer exposures, from 10 to 60 s.

A very tricky problem of advanced sky surveys is the fill factor, which is the ratio between the active portion of the focal plane and its total area. The assumed Fly-Eye telescope has the cameras well separated with a private focal plane segment for each one, resulting in a correlated fill factor exactly 1. Moreover, commercial chips with fill factor greater than 0.99 are available, thus we could avoid to consider the fill factor in the simulation, by assuming it very close to 1. Each pixel of the CCD sensors corresponds to 1.5 x 1.5 arcsec on the celestial sphere, thus an image has 256 Megapixels.

Another assumption concerns the image processing software. Instead of being based upon the identification of the individual pixels with high enough signal to noise ratio S/N, it is thought to specifically detect trailed images, by summing the readings along all possible lines in the frame, thus allowing to detect trails with S/N on each pixel even less than 1. Algorithms with this capability exist, have acceptable computational complexity and have been tested [11]. The actual implementation in operational software and field testing is an assumption. We assumed also to be able to reduce astrometrically the observations in an accurate way, with RMS error of 0.4 arcsec when the pixel S/N is good. When the RMS grows to more than 2 arcsec, see (3) below, orbit determination failure can occur.

A very critical observing parameter for a debris is the phase angle. To our knowledge, there is no calibration of the magnitude dimming due to the phase angle for space debris, while there is such a function for asteroids [3]. In our simulations the official IAU magnitude system, called H-G system, was used. We assumed a scheduler capable of taking into account the geometry of light and the phase, chasing the lowest possible phase out of the Earth shadow.

POPULATION MODEL

In order to produce a realistic simulation of the whole observation process a suitable population of orbiting objects is required. A subset of the ESA-MASTER2005 population, upgraded with the recent in-orbit collisions (FengYun-1C, IRIDIUM 33 - COSMOS 2251) was provided by ESOC. The MASTER model contains the largest objects taken from the USSTRATCOM Two Line Elements plus smaller objects generated with ad hoc source models. The population file did not contain any value for the albedo of the objects, a quantity that is needed to derive the magnitude of the object in the sky. From the available literature [1,9], a commonly accepted value of the albedo for a generic spacecraft is between 0.1 and 0.2. Therefore we made the conservative assumption of albedo 0.1 for all the objects. The absolute magnitude was derived according to the IAU standard for asteroids. The formula is $H = 33 - 5 \log_{10}(d)$, where d is the diameter of the object in m, provided by the MASTER file.

SNR MODEL

For each simulated observation the signal to noise ratio S/N expected at the observatory station performing the observation was computed, according to the following statistical model. Equations (2) are the formulas used for the computation of the S/N respectively for a starry source, a single pixel and an entire trail:

$$\frac{S}{N}_{star} = \frac{S}{\sqrt{S+N}}; \quad \frac{S}{N}_{pixel} = \frac{S/T}{\sqrt{S/T+N}}; \quad \frac{S}{N}_{trail} = \frac{S}{\sqrt{S+NT}}, \tag{2}$$

where T is the number of pixels trailed in the camera field during the exposure time. In this expressions N includes all the contributions from the sources of noise: the readout noise, the dark current noise and the sky background; the other term under square root accounts for the Poisson statistics. The expected signal is determined as a function of the object apparent magnitude, given the instrumental and observation parameters. The S/N for a single pixel is given by dividing the total signal of the debris by T. In this context, N is the noise in a single pixel, while in the formula for a star N is spread in few pixels, depending on the point spread function of the starry object. The algorithm described in [11] is capable to detect very faint trails, thanks to its capability of adding the signal along the trail direction. The resulting S/N formula for the entire trail is obtained by adding the signal belonging to all the pixels of the trail. This gives a contribution in the noise proportional to $T^{1/2}$. We used $S/N_{trail} \geq 6$ as a criterion for the detectability of a trail, in order to avoid false detections.

When the detected trail is too faint, the problem is to determine its beginning and end with high accuracy. In this case the astrometric error Z can be computed by

$$Z\frac{S}{N}_{pixel} \leq \sqrt{Z} \quad \rightarrow \quad Z = \left(\frac{1}{S/N_{pixel}}\right)^2. \tag{3}$$

In practice there are two regimes for the astrometric error. When the signal is strong, the astrometric error is dominated by the astrometry method, that is by the systematics in the astrometric catalogues. When the signal is weak, it is determined by (3).

Fig. 2 shows the curves of the S/N as function of the apparent magnitude for different cases. The blue line represents the case of a fixed star (no trailing), while the red lines correspond to a LEO object at 1400 km of altitude, respectively when the number of pixels T is minimum (T=200, solid red line) and when it is maximum (T=600, dashed red line). The plot also shows the degradation of the astrometric performance for low S/N on a single pixel, due to the difficulty of determining the end of the trail. The green line, representing the S/N over a single pixel when T=200, changes colour (green → red) when the astrometric error, represented by the magenta line, becomes greater than 0.4 arcsec and it becomes black when the corresponding S/N_{trail} for T=200 (solid red line) becomes lower than 6, in which case the object cannot be imaged in survey mode.

CORRELATION AND ORBIT DETERMINATION

Given two or more sets of observations, the main problem is to identify which separate data belong to the same object (correlation problem). Thus the orbit determination problem needs to be solved in two stages: first different observational data need to be correlated, then an orbit can be determined. With the Keplerian integrals method, briefly described below, it is possible to compute an orbit starting from only two exposures, taken at different passes, which are on average distant 1 day, corresponding to several revolutions. Since we started from scratch, without any a priori information on the observed objects, for any couple of exposures we tried to compute a preliminary orbit, solution of a 2-body approximation, or possibly taking into account the second zonal spherical harmonic of the Earth geopotential. This step has a computational cost growing with the square of the number of observed trails.

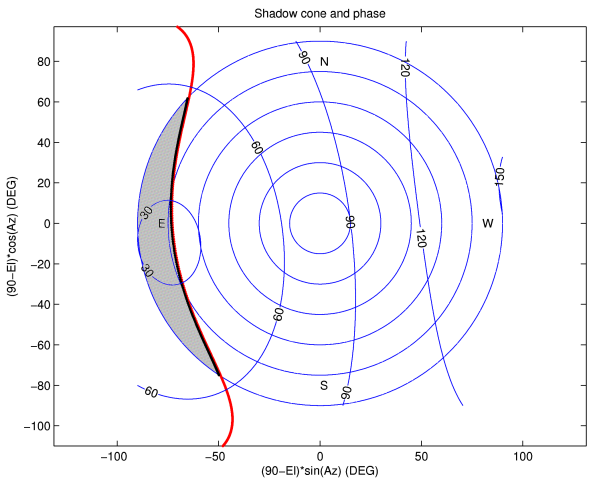

Fig. 1. Earth Shadow and iso-phase curves for a tropical station at local time 19 h on March 20th

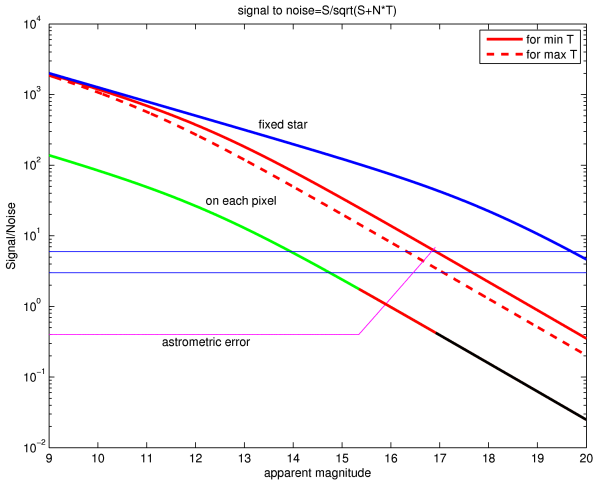

Fig. 2. Signal to noise ratio

The orbits obtained in this way have to be replaced by least squares orbits, with a dynamical model including all the relevant perturbations. To rule out the occurrence of false correlations we required at least 3 trails to accept an orbit. Thus 2-trails correlations needed to be confirmed by correlating further observations. This was done by the attribution procedure, which consists in trying to fit new observations to a known orbit, see [12, Sec. 7.6]. When an orbit is very well constrained and the number of involved trails is high enough, the possibility for the corresponding correlation to be false can be ruled out, by removing discordant correlations. In our simulations, if the correlation involved more than 3 trails, then the orbit could be considered reliable and the object was catalogued. When the number of fitting trails increased to 10, the object was numbered, by assigning a unique identifier (name).

The information related to a single object during an exposure can be summarized in an attributable, which is a 4-dimensional vector $A=(\alpha,\delta,\mathrm{d}\alpha/\mathrm{d}t,\mathrm{d}\delta/\mathrm{d}t)$, representing the angular position and velocity of the body at a time t. Usually α, δ are right ascension and declination. To compute a 6 parameters orbit, 2 further quantities, such as range and range rate (ρ, $\mathrm{d}\rho/\mathrm{d}t$), are needed. In our simulations we used the Keplerian integrals method to produce preliminary orbits from two attributables A_1, A_2 of the same object at two epoch times t_1 and t_2. The algorithm for the asteroid case is introduced in [8], while in [5] it is adapted to space debris. The 2-body energy E and the angular momentum $\boldsymbol{c}$ can be expressed as functions of A, ρ, $\mathrm{d}\rho/\mathrm{d}t$. By assuming the orbit between t_1 and t_2 well approximated by a Keplerian one, we have that

$$E(A_1,\rho_1,\dot\rho_1)-E(A_2,\rho_2,\dot\rho_2)=0\,,\quad \boldsymbol{c}(A_1,\rho_1,\dot\rho_1)-\boldsymbol{c}(A_2,\rho_2,\dot\rho_2)=0\,. \tag{4}$$

The above system can be reduced to a polynomial one in the two variables ρ_1,ρ_2, with total degree 48. By means of the resultant method from Computational Algebra, one of ρ_1,ρ_2 is eliminated, thus getting a univariate polynomial of degree 48. All positive real roots are computed by means of an optimized algorithm [2], so that all the solutions of (4) are finally obtained. By using the Keplerian approximation, compatibility conditions are imposed: the first one related to the perigee argument and the second one to the mean anomaly. The discrepancy from them is measured by a suitably defined norm χ. If such χ is smaller than a fixed threshold, the solution is accepted. The algorithm also provides a covariance matrix for the computed orbit. Typically less than 3 orbits remain after the entire procedure.

To deal with LEOs it is necessary to generalize the method, including the effect due to the Earth oblateness. The secular equations for Delaunay's variables ℓ, ω, Ω, $L=(\mu a)^{1/2}$, $G=L(1\text{-}e^2)^{1/2}$ and $Z=G\cos(I)$ are given by

$$\begin{gathered}\dot{\bar\ell}=n-\frac{3}{4}n\left(\frac{R_{Earth}}{a}\right)^2\frac{J_2\left(1-3\cos^2(I)\right)}{\left(1-e^2\right)^{3/2}}\,,\qquad \dot{\bar\omega}=\frac{3}{4}n\left(\frac{R_{Earth}}{a}\right)^2\frac{J_2\left(4-5\sin^2(I)\right)}{\left(1-e^2\right)^{2}}\,,\\ \dot{\bar\Omega}=-\frac{3}{2}n\left(\frac{R_{Earth}}{a}\right)^2\frac{J_2\cos(I)}{\left(1-e^2\right)^{2}}\,,\qquad \dot{\bar L}=\dot{\bar G}=\dot{\bar Z}=0,\end{gathered} \tag{5}$$

where J_2 is the coefficient of the second zonal spherical harmonic of the Earth gravity field, ℓ is the mean anomaly, ω is the perigee argument, Ω is the longitude of the ascending node, μ is the standard gravitational parameter of the Earth, a is the semimajor axis, e is the eccentricity, I is the inclination and $n=\mu a^{-3/2}$ is the mean motion. In this case we cannot use the conservation of angular momentum, since it precedes up to 5 $\cos(I)$ deg/day. Thus we consider the parametric problem obtained by imposing $\mathrm{d}\Omega/\mathrm{d}t=K$, with K constant:

$$E(A_1,\rho_1,\dot{\rho}_1)-E(A_2,\rho_2,\dot{\rho}_2)=0\,,\quad R\,\boldsymbol{c}(A_1,\rho_1,\dot{\rho}_1)-R^T\,\boldsymbol{c}(A_2,\rho_2,\dot{\rho}_2)=0\,, \tag{6}$$

where R is the rotation by $\Delta\Omega = K(t_2-t_1)/2$ around the vertical axis. Thus for a fixed value of K the problem has the same algebraic structure of the unperturbed one. The compatibility conditions contain the perigee precession and the secular perturbation in mean anomaly. The covariance matrix can be computed as well.

To solve system (6), we set up a fixed point iterative procedure as follows. First, we solve (6) for $K=K_0$, by selecting a value K_0 either using the circular orbits corresponding to each of the two attributables [6] or by assuming $K_0=0$. Among the obtained solutions, we cannot know which one could lead to convergence. Since the value of K_0 is quite arbitrary, it is not safe to select only those with a low value of χ. Thus we use all the solutions as possible starting guess for the iterative procedure. Given the orbital elements E_i at step i we compute the corresponding value of K by (5) and for the computed value of K we solve the corresponding system (6). We select the solution with the lowest value of χ and compute the corresponding orbital elements E_{i+1}. Then we keep iterating until convergence.

CATALOGUE BUILD-UP SIMULATION

We assumed to start with no information on the satellite and debris population in the region of interest (high LEO) and attempted to build up an orbit catalogue, to be compared with the MASTER one. For this purpose we conducted a large scale simulation, by choosing two different population samples, dubbed Population 1 and Population 2. Population 1 was made up of 912 objects, randomly selected among those with diameter between 8 and 27 cm, and with altitude of perigee h_p between 1300 and 2000 km. Population 2 included 1104 objects, with diameter between 5 and 25 cm, and with $1000 \le h_p < 1300$ km. Objects larger than 27 cm and 25 cm respectively were not included in the simulation, since the amount of observational data allows us to attain a complete catalogue in a comparatively short time span. This is confirmed not only by some preliminary tests but also by the analysis of this simulation, which shows that all the objects larger than 20 cm are catalogued within 1 month.

Fig. 3 shows two rectangles on the perigee altitude-diameter plane, which enclose the regions corresponding to the selected population samples. The choices of the population samples were driven by the hypothetical performances of an enhanced radar sensor, to be used along with the optical ones in the ESA-SSA program. For the considered values of the perigee altitude, we have drawn two curves, representing the observing capabilities of a baseline radar and of an enhanced one. These curves give the minimum diameter d_{min} of observable objects as function of the perigee altitude h_p. They are determined according to $d_{min} = (h_p/h_{ref})^2\, d_{ref}$, where h_{ref} and d_{ref} are reference values for the perigee altitude and the diameter, determined on the basis of the radar characteristics. We set $h_{ref} = 2000$ km and $d_{ref} = 32$ cm for a baseline radar, meaning that it is capable to observe almost all the objects with $h_p = 2000$ km and diameter down to 32 cm. For an enhanced radar we took $h_{ref} = 2000$ km and $d_{ref} = 20$ cm. The two rectangles cover the region lying above the curve of the enhanced radar. The results for both the population samples after 2 months of survey observations are reported. Resident LEOs are represented by points, objects in orbits transiting in the LEO region by circles. The green color means that the overall procedure succeeded in obtaining an orbit for the object, red that there were no observations and black that the observations did not suffice to obtain an acceptable orbit. The reasons for the occurrence of this last possibility are essentially two: the observations were very few and too distant in time, so that correlation was not possible; the observations had low accuracy, so that both the computation of an orbit or the attribution of further trails failed. Anyway, the presence of black dots is relevant only in the low region of Population 2. This means that, in the case of resident LEOs, the failure of catalogue build-up can happen only for some fast moving objects with diameter < 8 cm.

To analyse the results, we measured the efficiency of the catalogue build-up, defined as the ratio between the number of reliable orbits computed (with at least 3 trails) and the total number of sampled objects. The results for Population 1 were overwhelming. For $h_p \ge 1300$ km, we computed the orbits of almost all the objects above 8 cm (98.1%) and of 99.6% of resident LEOs. If we consider only the objects above the curve of enhanced radar performance in Fig. 3, then the total efficiency is 98.6%, while for resident LEOs it is 99.8%. A few objects in highly eccentric transit orbits (e.g., GTO) were lost, but they should be observed with a different strategy, such as non-sidereal tracking targeting them at apogee [13]. For Population 2 the total efficiency is 82.8%, while considering only resident LEOs it is 86.6%; if we take into account only the region above the curve of the enhanced radar the corresponding percentages are 93.7% and 98.9%. Moreover, the outcome of the two simulations suggests that the problem is not the altitude but the diameter: indeed, even for Population 2, among the objects larger than 8 cm, 95.8% had a reliable orbit, and for resident LEOs the percentage was 99.0%. Smaller debris require a larger telescope, whatever the height.

To get the big picture of the results, we should take into account also the biggest objects of the MASTER population. Moreover, the results of Population 1 have to be weighted twice, since we randomly selected only half of the objects. By assuming that all the biggest objects were catalogued after 2 months of survey, we get an overall efficiency 97.9% for the objects above the enhanced radar curve. By considering only LEOs the efficiency is 99.0%. Fig. 3 shows that

most of the difficulties in the catalogue build-up concern the region of orbital perigee altitude less than 1100 km. If we discard this region, the total efficiency reaches 98.9%, and for LEOs 99.8%.

ORBIT IMPROVEMENT PHASE

Tasking observations are possible if, by moving the telescope at non-sidereal rate, the object remains in the telescope field of view. Moreover, it is desirable to see the object with most signal concentrated on a single pixel, thus obtaining a higher signal with respect to the survey mode. We considered the numbered objects obtained after 1 month and we propagated the orbits for 1 week after the last observation. Then the angular error in prediction and the relative error in angular velocity were computed. Taking into account that the angular velocity of the objects in our sample was less than 2000 arcsec/s, to see the object in a single pixel during tasking the relative error in angular velocity had to be less than 7.5×10^{-4}. This was achieved for all the numbered objects. Moreover the angular error in position was always less than 95 arcsec. Then the possibility of follow-up was confirmed and we were allowed to take T=1 (no trailing loss) in the S/N formula.

In this phase, we chose the same two population samples used for the survey step, but we excluded high eccentricity transit LEOs, since the observation strategy was not suitable for this kind of objects, as confirmed by the results of the catalogue build-up. At the starting time of the simulation, the sampled objects were assumed to be catalogued with sufficiently well determined orbits. The same procedure of the survey simulation was adopted, meaning that the previously computed catalogue was not used and the orbit determination was performed again from scratch. The difference was in the kind and the amount of data, as follow up observations were more numerous and accurate than the survey ones.

The orbit improvement goal was defined by choosing an accuracy envelope to which compare the accuracy of the computed orbits. First we fixed the object-centred reference frame $\{\mathbf{u},\mathbf{v},\mathbf{w}\}$, where $\mathbf{u}$ is the direction from Earth centre to the object centre, $\mathbf{w}$ is the direction of the angular momentum vector and $\mathbf{v} = \mathbf{w} \times \mathbf{u}$. Then the accuracy ellipsoid in position for resident LEOs was 4, 30, 20 m along the directions $\mathbf{u},\mathbf{v},\mathbf{w}$ respectively, for transit object it was 10, 60, 200 m. The accuracy ellipsoid in velocity was 20, 4, 20 mm/s both for resident LEOs and transit objects. These ellipsoids were derived from collision avoidance requirements. The simulation covered three weeks of tasking. All the numbered orbits were propagated for 1 week after the last observation and compared to the accuracy envelope. The comparison was performed through a suitably defined norm, called accuracy envelope norm, which is ≤ 1 whenever the uncertainty is smaller than the envelope.

Fig. 4 shows the results after 3 weeks. The numbered objects are drawn on the perigee altitude-diameter plane. The points are resident LEOs, circles are transit objects. Green indicates that both the accuracy norms in position and velocity are ≤ 1. Black means that one of them is > 1 and both are ≤ 2. Red means that at least one of them is >2. The prevalence of the green colour means that for almost all the numbered objects, both the accuracy norms are ≤ 1. Indeed, for Population 1, 99.5% of resident LEOs and 100% of transit objects satisfy the envelope both in position and velocity. For Population 2, the percentages are 99.9% for resident LEOs and 74.5% for transit objects. Anyway, for transit objects the results are not statistically representative, because in both population samples they were less than 100 objects. Finally, it must be stressed that the relative error in velocity prediction was always less than 10^{-4}. Then with tasking observations there is no trailing loss and the observations always remain concentrated on a single pixel.

FRAGMENTATION DETECTION

A particular demanding situation for a surveillance network occurs whenever a fragmentation happens in Earth orbit. The resulting cloud of fragments can pose significant immediate or short term risks for other space assets in the same orbital region [14]. Therefore we simulated the fragmentation of a satellite due to both an explosion and a catastrophic collision. To produce the cloud of fragments we used, for both cases, the ISTI-CNR implementation of the NASA-JSC model [10]. According to the model, each fragment was characterized by the following elements: size d, mass, area, ΔV. From the whole cloud of fragments, we selected only those objects with $d > 10$ cm and $\Delta V < 100$ m/s, that is we focused on the core of the cloud. Given the Cartesian coordinates of the parent body, the isotropic ΔV relative to each fragment was added to these coordinates, thus obtaining the state vector of each fragment. The orbital elements of the fragments were then propagated for 21 days and survey observations were simulated.

First we simulated the explosion of a satellite with mass of 1000 kg. The satellite was supposed to be on a circular orbit at 1400 km of altitude, with an inclination of 74 deg. The model produced a cloud of 175 fragments with the above characteristics. Within these fragments, 8 had $\Delta V < 10$ m/s. In the first day after the explosion it was not possible to detect any debris, while, in the second and in the third day, about half of the debris were detected (26.3% in the second day, 57.7% in the third day and already 98.9% in the fourth day). This situation depends on the fact that in the first day the fragments cloud had still a non-homogeneous distribution around the Earth. The debris created by the explosion formed a cloud concentrated around the explosion point.

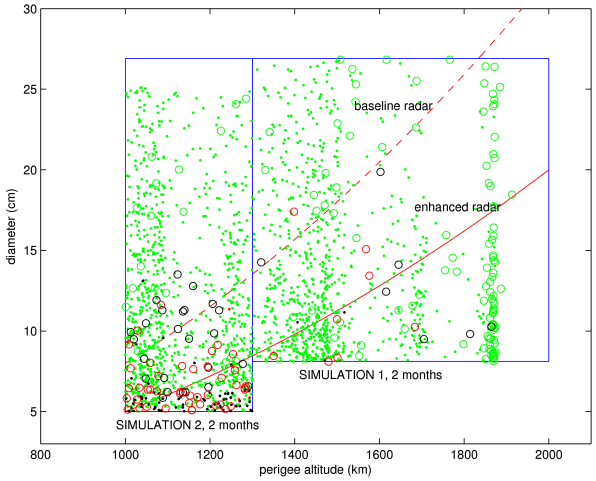

Fig. 3. Results of catalog build-up after 2 months

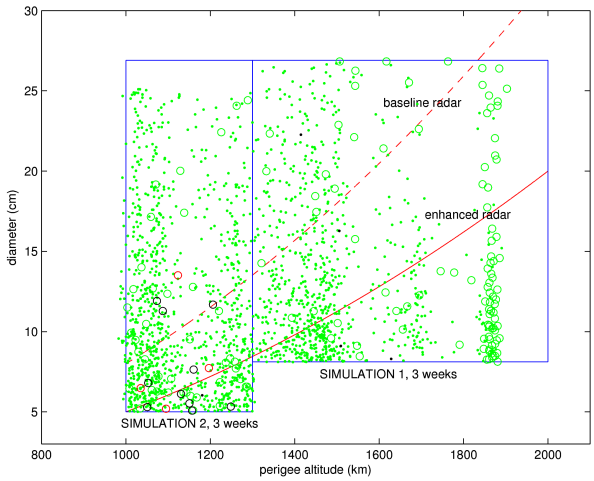

Fig. 4. Accuracy after 3 weeks of tasking observations

Therefore, in the first hours after the event, the detection of the concentrated cloud was similar to the detection of a single object. If the cloud was not passing in the right moment of the night above a station with favourable meteorological conditions, its detection was not possible. On the contrary, a few days after the explosion, all the debris were detected because they had a homogeneous distribution in a torus around the parent body orbit. It is therefore important to remind that the debris detection after a fragmentation depends on the ground station meteorological data. In particular, in the first day only 2 ground stations were able to observe, but the debris cloud was not passing above these stations.

In the second simulation, the collision of a debris with a mass of 10 kg against a satellite with mass of 1000 kg, with an impact velocity of 9 km/s, was simulated. In the NASA model, a collision is considered catastrophic whenever the ratio between the kinetic energy of the projectile and the mass of the target exceeds 40000 J/kg. This condition is largely satisfied by our event, so we are considering a catastrophic collision. The target satellite was supposed to be on the same orbit as in the explosion case. The model produced a cloud of 393 fragments with $d > 10$ cm and $\Delta V < 100$ m/s. Within these fragments, 7 had $\Delta V < 10$ m/s. The evolution of the cloud of fragments is similar to the one discussed in the explosion case and even the detection statistics (33.6% detected objects in the second day, 57.7% in the third day, 66.4% in the fourth day and 99.7% in the fifth day).

After simulating the observations performed by the ground network, we started the correlation and orbit determination process, to check how long it takes to get robust information on the fragmentation. Clearly, if 2 days were enough to observe a quite high percentage of fragments, they were not enough to compute also reliable orbits for the observed fragments. There were too few observations and in fact no orbits were available after only two days for both the simulations. After 4 days the situation improved and 90 orbits for the collision fragments and 46 orbits for the explosion fragments were computed, if we considered as acceptable correlations of at least 3 trails and discarded the ones between only 2 trails. By comparison with the ground truth we found that some of the correlations were false, that is they put together observations of different objects. Anyway, all the false correlations had only 3 trails and this was true for both the simulations in the entire period examined. Note that, in the case of the fragments clouds, it is quite natural to have false correlations even among 3 trails, because all the fragments have very similar orbits. To exclude false correlations, in this peculiar case, we had to consider only orbits fitting at least 4 trails. In our analysis we considered as reliable the orbits with at least 5 trails and numbered the orbits with at least 10 trails. We found that, after only 2 weeks, all the objects were numbered both in the explosion and in the collision case.

The graphical tool commonly used to characterize an in-orbit fragmentation is the Gabbard diagram, which is a plot of the apogee/perigee height of the fragments as a function of their orbital period. Fig. 5 shows the Gabbard diagram for the collision case, six days after the event. The X-shape, a typical signature of a fragmentation, is already visible.

CONCLUSIONS

The results of the catalogue build-up simulation show that more than 98% of the LEO objects with perigee height above 1100 km and diameter greater than 8 cm can be catalogued in 2 months. As Fig. 3 shows, a central area around 1100 km of orbital perigee altitude has been identified where the radar and the optical network should operate in a cooperative way. All the numbered orbits are accurate enough to allow follow-up observations with no trailing loss, and the orbit accuracy from the improved orbits is compliant with the collision avoidance requirements. Finally the simulated network of telescopes is able to detect and catalogue the fragments generated by a catastrophic event just a few days after the event.

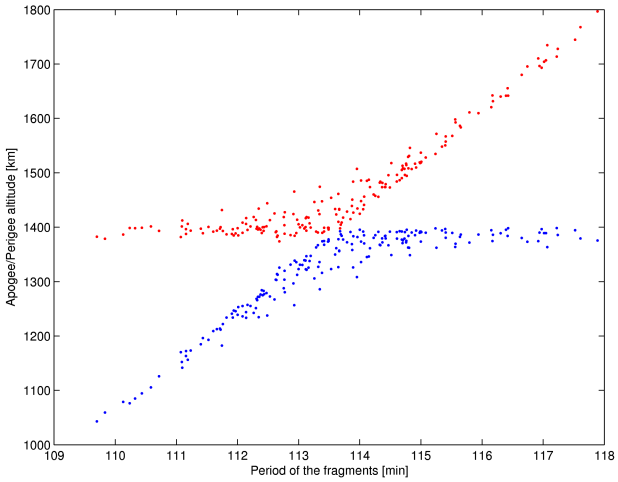

Fig. 5. Collision fragments with reliable orbits after 6 days. Red: apogee; Blue: perigee

AKNOWLEDGEMENTS

We wish to thank CGS for providing us with the expected sensor performances and realistic simulated observations, taking into account the characteristics of the Fly-Eye telescope, the meteorological model to account for cloud cover, and the statistical model for the signal to noise ratio. This work was performed under ESA/ESOC contract 22750/09/D/HK SARA-Part I *Feasibility study of an innovative system for debris surveillance in LEO regime*, with CGS as prime contractor.

REFERENCES

[1] J.L. Africano, E.G. Stansbery, and P.W. Kervin, "The optical orbital debris measurement program at NASA and AMOS," *Advances in Space Research*, vol. 34/5, pp. 892-900, 2004.
[2] D.A. Bini, "Numerical computation of polynomial zeros by means of Aberth method," *Numerical Algorithms*, vol. 13/3-4, pp. 179-200, 1997.
[3] E. Bowell, B. Hapke, D. Domingue, K. Lumme, J. Peltoniemi, and A.W. Harris, "Application of photometric models to asteroids," *Asteroids II*, The University of Arizona Press, 1989.
[4] L. Cibin, P.M. Besso, M. Chiarini, A. Milani Comparetti, and A. Ragazzoni, "Debris telescopes catch objects in Leo zone," *IAC-10-A6.5.10*, 2010.
[5] D. Farnocchia, G. Tommei, A. Milani, and A. Rossi, "Innovative methods of correlation and orbit determination for space debris," *Celest. Mech. Dyn. Astr.*, vol. 107/1-2, pp. 169-185, 2010.
[6] K. Fujimoto, J.D. Maruskin, and D.J. Scheeres, "Circular and zero-inclination solutions for optical observations of Earth-orbiting objects," *Celest. Mech. Dyn. Astr.*, vol. 106, pp. 157-182, 2010.
[7] K.F. Gauss, *Teoria motvs corporvm coelestivm in sectionibvs conicis solem ambientivm*, Hambvrgi, Svmtibvs F. Perthes et I.H. Besser, 1809.
[8] G.F. Gronchi, L. Dimare, and A. Milani, "Orbit determination with the two-body integrals," *Celest. Mech. Dyn. Astr.*, vol. 107/3, pp. 299-318, 2010.
[9] D.J. Kessler, and K.S. Jarvis, "Obtaining the properly weighted average albedo of orbital debris from optical and radar data," *Advances in Space Research*, vol. 34/5, pp. 1006-1012, 2004.
[10] N.L. Johnson, P.H. Krisko, J.-C. Liou, and P.D. Anz-Meador, "NASA's new breakup model of evolve 4.0," *Advances in Space Research*, vol. 28, pp. 1377-1384, 2001.
[11] A. Milani, A. Villani, and M. Stiavelli, "Discovery of very small asteroids by automated trail detection," *Earth, Moon, and Planets*, vol. 72, pp. 257-262, 1996.
[12] A. Milani, and G.F. Gronchi, *Theory of orbit determination*, Cambridge University Press, 2010.
[13] A. Milani, G. Tommei, D. Farnocchia, A. Rossi, T. Schildknecht, and R. Jehn, "Orbit determination of space objects based on sparse optical data," unpublished.
[14] A. Rossi, G.B. Valsecchi, and P. Farinella, "Risk of collision for constellation satellites," *Nature*, vol. 399, pp. 743-744, 1999.